Cai *et al. Int J Concr Struct Mater* (2019) 13:46
https://doi.org/10.1186/s40069-019-0358-8

International Journal of Concrete Structures and Materials

RESEARCH Open Access

Shear Resistance Prediction of Post-fire Reinforced Concrete Beams Using Artificial Neural Network

Bin Cai[1,2], Long-Fei Xu[1] and Feng Fu[2*]

Abstract

In this paper, a prediction method based on artificial neural network was developed to rapidly determine the residual shear resistance of reinforced concrete (RC) beams after fire. Firstly, the temperature distribution along the beam section was determined through finite element analysis using software ABAQUS. A residual shear strength calculation model was developed and validated using the test data. Using this model, 384 data entries were derived for training and testing. The input layer of neural network involved parameters of beam height, beam width, fire exposure time, cross-sectional area of stirrup, stirrup spacing, concrete strength, and concrete cover thickness. The output was the shear resistance of RC beams. It was found that use of BP neural network could precisely predict the post-fire shear resistance of RC beams. The predicted data were highly consistent with the target data. Thus, this is a novel method for computing post-fire shear resistance of RC beams. Using this new method, further investigation was also made on the effects of different parameters on the shear resistance of the beams.

Keywords: reinforced concrete, fire, shear resistance, sectional analysis, BP neural networks

1 Introduction

When fire occurs, reinforced concrete (RC) beams are affected by high temperatures and their mechanical properties are significantly deteriorated with the temperature rise (Felicetti et al. 2009; Annerel and Taerwe 2011). The parameters needed for computing the shear resistance of post-fire RC beams include fire exposure time, specific heat, temperature distribution, section sizes and material strength. However, numerous computations steps are needed to determine shear resistance. On the contrary, neural network algorithms can predict accurate shear resistance and thereby avoid complex computation (Erdem 2015).

Artificial neural networks (ANNs) can be extensively applied in optimization, signal processing, pattern recognition, and intelligent control owing to their strong nonlinear analysis ability. Kurtgoz et al. (2018) evaluated the performance of methane engines using ANN. Gupta et al. (2017) used ANN to measure SpO2 of clinical management systems. Mossalam and Arafa (2017) designed an instrument panel using ANN. Viotti et al. (2002) used ANN to study the air pollution in cities. Lesniak and Juszczyk (2018) used ANN to predict indirect field fees. Sarro et al. (2003) used ANN to automatically classify light curves. The above studies largely contribute to the research on ANN.

ANN has also been widely applied into engineering and used by many researchers to solve practical engineering problems. Abbasi and Hogg (2005) built a glass fiber-reinforced steel concrete beam prediction model, predicted the effects of fire exposure time on RC beams, and found the failure mode of the predicted beams was steel fracture. Chowdhury and Bisby (2008) studied the concrete T-shaped beams reinforced with fiber-enhanced polymers and found the post-fire FRP-reinforced concrete beams reserved the bending bearing capacity before the reinforcement. Keskin

*Correspondence: cenffu@yahoo.co.uk
[2] School of Mathematics, Computer Science and Engineering, City, University of London, London, UK
Full list of author information is available at the end of the article
Journal information: ISSN 1976-0485 / eISSN 2234-1315

and Arslan (2013) studied the anti-cracking strength of non-stirrup reinforced concrete beams and found ANN outperformed equations from six code, and the equations proposed by 12 different researchers. Ožbolt et al. (2014) discussed the numerical computations of RC beams at high temperature and machinery loading and found ANNs could successfully predict the machinery loads during and after fire exposure. Erdem (2010) predicted the post-fire bending bearing capacity of RC plates and found the ANN model could precisely predict the ultimate bending moment ability of post-fire RC plates within the ranges of the inputted parameters. Bengar et al. (2016) predicted the ductility of RC beams and found ANN could modestly and precisely predict the curvature ductility of RC beams. Naser et al. (2012) analyzed the fire-resistance of CFRP plate-reinforced concrete T-shaped beams during fires and found the ANN-predicted results and tests were highly correlated with the FE results, indicating the ANN can be used to predict the mechanical properties of these reinforced beams. Mashrei et al. (2010) used a BP neural network model to predict the bending moment ability of steel wire network components and found this model predicted excellent results. However, ANN has been rarely used to study the post-fire shear resistance of RC beams.

Thus, in this study, a method was proposed for fast prediction of the post-fire shear resistance of RC beams. Firstly, temperature distribution of the beams was determined using the finite element analysis software ABAQUS, and the strength reduction factor of materials was detected. Then the post-fire shear resistance of RC beams was calculated via section equilibrium analysis. The accuracy of the post-fire shear resistance reduction model was validated using the test data, the model was used to produce the required learning and training data for machine learning. The post-fire shear resistance of RC beams was predicted using machine learning based on BP neural networks. The data predicted by the machine were compared with the target data, sufficient accuracy was achieved by of ANN.

2 Post-fire Shear Resistance Reduction Model

2.1 Fundamental Heat Transfer Analysis Theory (Fu 2016)

2.1.1 Conduction (Yang 2008)

In the steady-state situation, the transfer of heat by conduction can be calculated as follows:

$$q = kdT/dz \tag{1}$$

where q is the heat flow per unit (W/m^2), k is the thermal conductivity, T is the temperature, z is the distance in the direction of heat flow.

2.1.2 Convection (Liu et al. 2000)

Convection is the heat transfer by the movement of fluids, either gases or liquids. It can be calculated as follows:

$$q = h_c \Delta T \tag{2}$$

where h_c is the convective heat transfer coefficient (W/m^{2}K), ΔT is the temperature difference between the surface of the solid and the fluid.

2.1.3 Radiation (Zhu 2011)

Radiation is the transfer of the energy by electromagnetic waves. It is extremely important in fire as it is the main mechanism for heat transfer. It can be decided as follows:

$$q = \varphi \varepsilon \sigma (T_e^4 - T_r^4) \tag{3}$$

where φ is the configuration factor, ε is the surface emissivity, σ is Stefan-Boltzmann constant (5.67×10^{-8}W/m2K4), T_e is the absolute temperature of emitting surface (K), T_r is the absolute temperature of receiving surface (K).

2.2 Temperature Distribution of Beams Under Fire

When determine the shear resistance of beam under fire, only maximum temperature of beams at different locations is needed, therefore, the ISO834 fire curve (ISO 1999) was used here, and the temperature–time relation could be expressed as follows:

$$T = T_0 + 345 \lg (8t + 1) \tag{4}$$

where T_0 is the room temperature, and t is the heating time. The standard fire curve was shown in Fig. 1.

The temperature distribution of post-fire beams was numerically simulated using general purpose software ABAQUS. The concrete was simulated using three-dimensional entity heat conduction element C3D8R, and the steel reinforcement is simulated using T3D2-Truss element. The thermal parameters of reinforcement and concrete were both determined from Eurocode (BSI

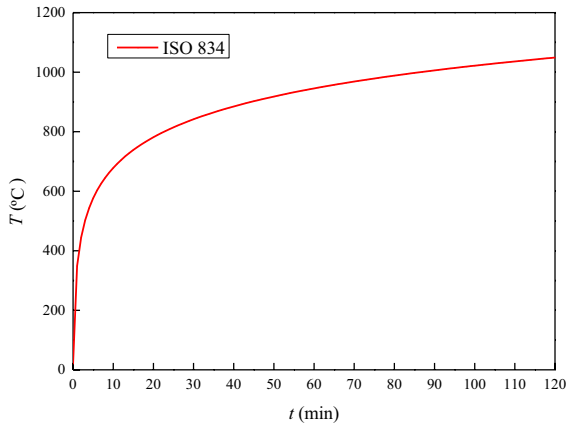

Fig. 1 The standard fire curve specified in ISO 834.

2004, 2013). The concrete and reinforcement were bound together using *Tie command available in ABAQUS, and the mesh size was 0.04 m. Thereby, temperature distribution across the beam section exposed to fires at three sides was determined. The method considers the strength reduction of each small unit on the section, which has a higher precision. The strength calculation formula is based on the Chinese concrete code GB50010-2010, which does not consider the influence of the longitudinal reinforcement. The fire exposure time was 60, 90 and 120 min. The temperature calculation model and its mesh division were shown in Fig. 2.

In order to validate the accuracy of the thermal response simulation, this model was applied to determine the temperatures at sectional points 1 to 5 in Ref. (Xu et al. 2013). The positions of the 5 temperature measuring

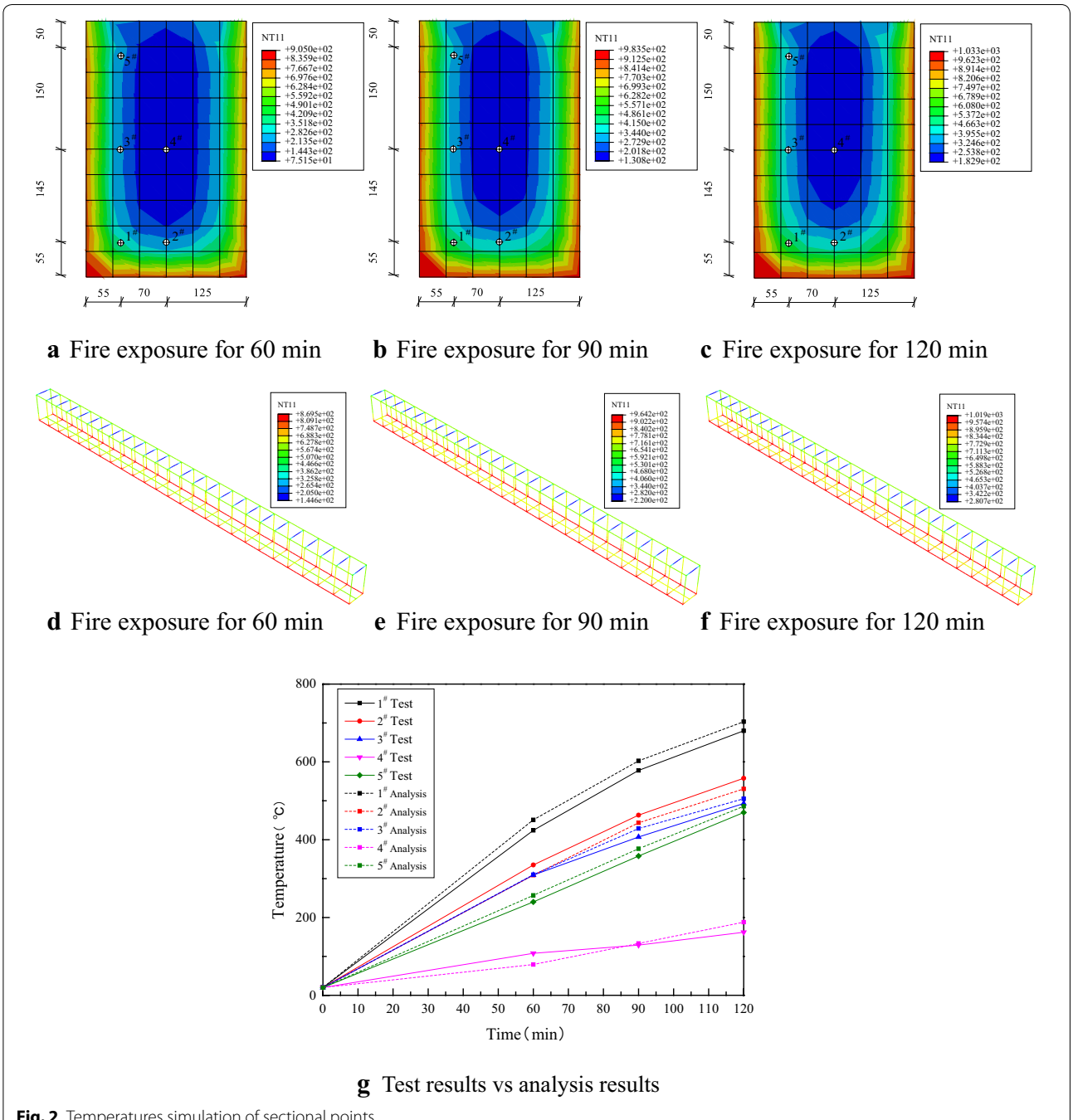

Fig. 2 Temperatures simulation of sectional points.

points and the analysis temperature vs time relations were shown in Fig. 2a–c. The temperature distribution of the steel reinforcement is shown in Fig. 2. Since the RC beam is exposed to fire on three sides, the stirrup is heated evenly, so the average temperature is taken as the stirrup temperature. The analysis results by ABAQUS and test results by experiments were shown in Fig. 2g. Concrete is slow in heat transfer (Yu et al. 2012). During initial heating, the moisture in the concrete absorbs heat and evaporates, and the interior of the concrete heats up slowly. The temperatures at all points were marching well, indicating the temperature distribution simulated by ABAQUS were correct and effective.

2.3 Tensile Strengths of Concrete and Reinforced Steel After Fire

The concrete tensile strength reduction factor at the corresponding temperature can be expressed as follows (Hu et al. 2014):

$$\varphi_{\mathrm{tT}} = \frac{f\mathrm{t}(T)}{f\mathrm{t}} = 0.976 + \left[1.56 \times \left(\frac{T}{100}\right) - 4.35 \times \left(\frac{T}{100}\right)^2 + 0.345 \times \left(\frac{T}{100}\right)^3\right] \times 10^{-2} \tag{5}$$

where $f\mathrm{t}(T)$ is the tensile strength of post-fire concrete at T °C, $f\mathrm{t}$ is the tensile strength of concrete at normal temperature, and φ_{tT} is the tensile strength reduction factor of post-fire concrete.

The yield strength reduction factor φ_{yvT} of reinforced steel at the corresponding temperature can be determined from Ref. (Molkens et al. 2017) (Table 1).

2.4 Computation of Residual Resistance Based on Section Equilibrium

A section equilibrium method is developed here based on several existing literatures (El-Fitiany and Youssef 2017; Erdem 2015), which utilize the heat transferring result from the FE analysis. Therefore, it is believed to be a more accurate method to calculate the residual shear strength. The beam section is shown in Fig. 3 with the size of the finite element mesh displayed. Based on the temperature distribution across the beam section obtained from the finite element analysis, the tensile strength reduction factor of concrete beam can be calculated using the section equilibrium method. In this method, the section is divided into equal height rectangular cross section, and correspondent stress blocks can be obtained, therefore:

$$\bar{\varphi}_{\mathrm{tT}} = \frac{\sum \varphi_{t\mathrm{Ti}} \Delta b \Delta h}{bh} \tag{6}$$

where $\varphi_{t\mathrm{Ti}}$ is the concrete tensile strength reduction factor in the i-th zone of the component section, b is the width of beams, h is the height of beams, Δb is the unit width, and Δh is the unit height.

The tensile strength reduction factor of stirrup can be computed as follows:

$$\bar{\varphi}_{\mathrm{yvT}} = \frac{\sum \varphi_{\mathrm{yvTi}}}{n} \tag{7}$$

where $\bar{\varphi}_{\mathrm{yvT}}$ is the tensile strength reduction factor of stirrup, φ_{yvTi} is the tensile strength reduction factor at the temperature of the i-th point, n is the number of temperature distribution points on the stirrup.

Using the above deduction factor, the post-fire shear resistance of RC beams can be computed as (GB 2010):

$$V_{\mathrm{T}} = \alpha_{cv} \bar{\varphi}_{t\mathrm{T}} f_t b h_0 + \bar{\varphi}_{\mathrm{yvT}} f_{\mathrm{yv}} \frac{A_{\mathrm{sv}}}{s} h_0 \tag{8}$$

Where α_{cv} is the Shear bearing capacity coefficient of inclined plane.

Table 1 The yield strength reduction factor of reinforced steel.

T [°C]	φ_{yvT}
20	1.00
50	1.00
100	1.00
200	1.00
400	1.00
550	1.00
600	1.00
700	0.70
850	0.60

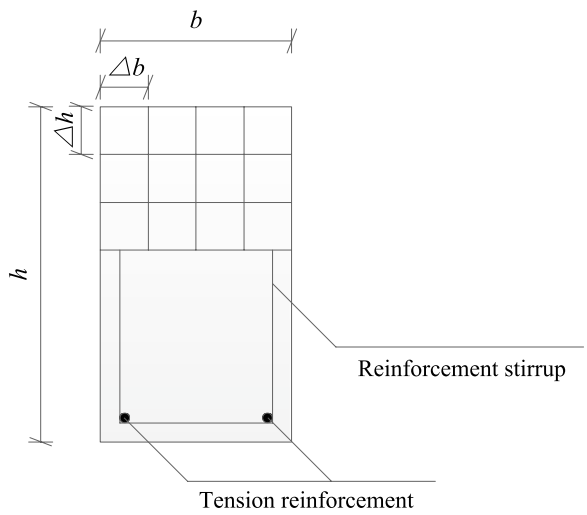

Fig. 3 Element division of post-fire beam sections.

α_{cv} is 0.7; h_0 is the efficient sectional beam height, A_{sv} is the sectional area of single-limb of stirrup; s is the stirrup spacing, $f$yv is the tensile strength of stirrup at normal temperature, VT is the shear resistance of RC beams at the post-fire temperature T °C.

L5 in Ref (Xu et al. 2013) is used for validation. The calculated flexural capacity of L5 beam after 60 min of fire is 201.53 kN m, and the residual flexural capacity of L5 in Ref (Xu et al. 2013) is 196 kN m. The calculation results are close to the experimental results. In the Ref (Xu et al. 2013), the initial flexural capacity of L5 beam before fire was 216 kN m, and the flexural capacity after 60 min of fire was 196 kN m. After the fire test, the flexural capacity decreased 10.2%. It shows that it is accurate to calculate the shear capacity and flexural capacity by this method.

2.5 Verification of Proposed Calculation Method for Shear Resistance of Post-fire RC Beams

The post-fire shear resistance calculation model of RC beams was validated using the test data in Ref. (Xu et al. 2013; Xu et al. 2015), and the concrete reinforcement of the specimen is illustrated in Fig. 4a, b. The flow chart for the shear resistance of post-fire RC beams is shown in Fig. 5. The temperature distribution was simulated using ABAQUS to determine the temperatures of RC beams and stirrup. With Eqs. (5) and (6), the tensile strength reduction factor of sectional concrete post-fire beams was determined. With Table 1 and Eq. (7), the tensile strength reduction factor of stirrup was determined. The shear resistance of specimen L9 was calculated with Eq. (8) and sectional analysis to be 125 kN, with error 4.2% from that (120 kN) of specimen L9 in Ref. (Xu et al. 2013). The shear resistance of specimen L4 was calculated to be 142 kN, with error 3.4% compared to that (147 kN) of specimen L4 in Ref. (Xu et al. 2015). The shear resistance determined from the new strength reduction model was well consistent with the fitted data in Ref. (Xu et al. 2013) and Ref. (Xu et al. 2015), indicating this method can be accurately and effectively used to compute the post-fire shear resistance of RC beams. This verification method is only applicable to RC beams heated in accordance with the ISO834 specification.

3 Artificial Neural Network (ANN)

ANN is a self-organized, self-learning and self-adaptive nonlinear artificial intelligence information processing system that is an interconnection of numerous

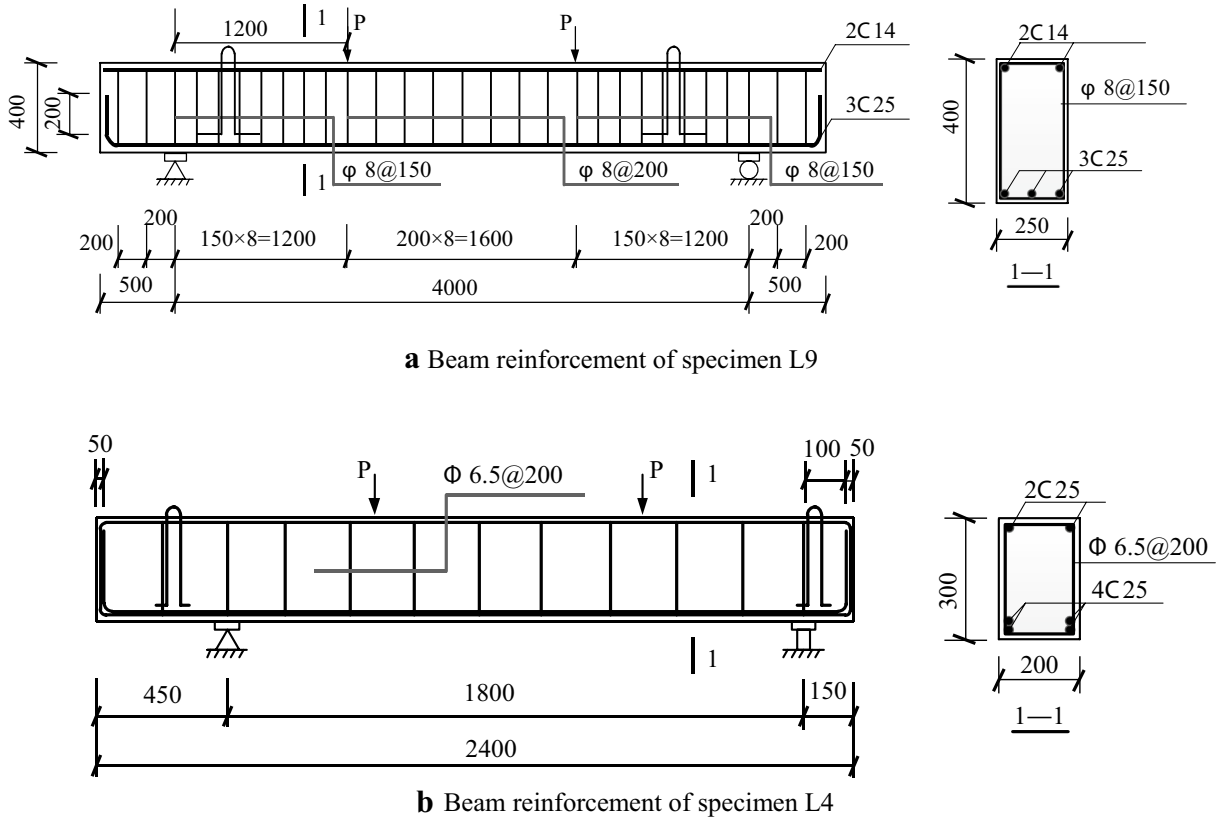

Fig. 4 Beam reinforcement of specimen.

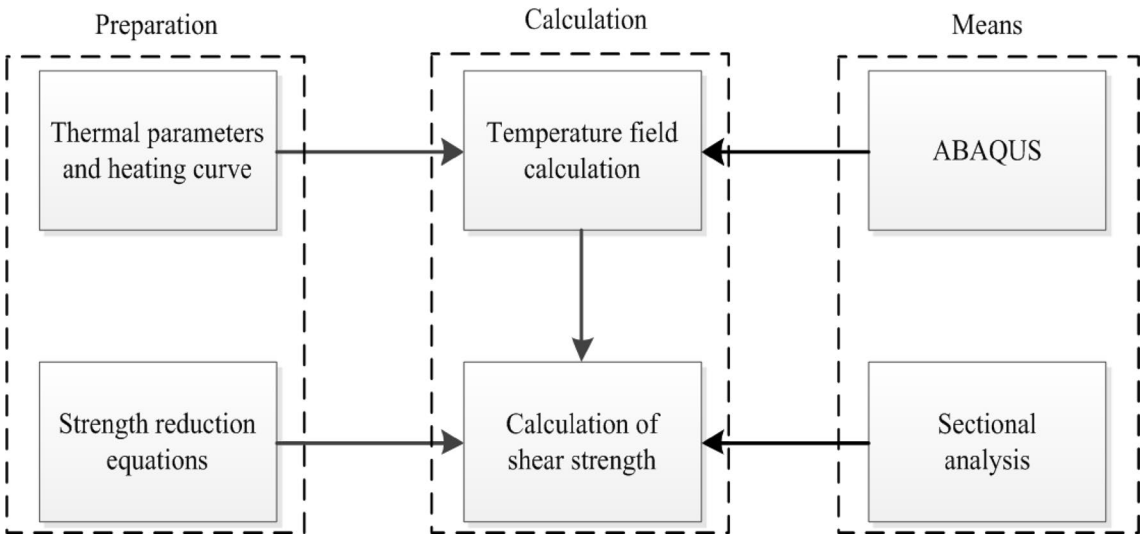

Fig. 5 Simulation procedure for the shear resistance of post-fire RC beams.

processing units (Marugán et al. 2018). ANN is based on modern nerve science and simulates the cerebral processing mechanism to achieve the simulated effect by simulating the basic characteristics of biological nervous systems. ANN is usually called an array of highly connected neurons, and the preset input can be mapped to the expected output after a number of simple basic units are trained by interconnection (Staub et al. 2015). Each neuron has a simple structure and function, but the system organized by numerous neurons is very complicated. With a very strong nonlinear processing ability, ANN can use some existing test data to spontaneously find out the nonlinear relation between the input and output without any artificially inputted equation, and returns a mathematical model that can map the inner relations of the test data (Zhou and Ke 2016). BP neural network proposed by Rumelhart and McCelland in 1986 is a multilayer forward network trained by the BP algorithm (Rumelhart et al. 1986). BP neural network is one of the most widely used neural network models. The process includes forward propagation of information and back propagation of errors (Lou et al. 2017). It exhibits excellent generalization ability, good fault tolerance and good ability to learn new knowledge. The learning rule of BP neural network is to use the gradient descent method to continuously adjust the weight and threshold of the network through back-propagation to minimize the sum of squared errors of the network. The topological structure of the multilayer forward model in one BP neural network consists of an input layer, a hidden layer and an output layer. The learning algorithm learns by using the input and output data from the target. The mean square error (MSE) function is a linear neural network performance function. The correlation coefficient (R) measures the degree of linear correlation between variables and can be used to regress two variables or more. MSE and R can be used to evaluate the precision of networks.

Mean Square Error expression between target data and predicted data of the network can be computed as follows:

$$E = \frac{1}{N}\sum_{i=1}^{N}(y_i - \hat{y}_i)^2 \tag{9}$$

where N is number of samples, y_i is target data, $\hat{y}_i$ is predicted data.

4 Shear Resistance Predicted by BP Neural Networks

4.1 Input and Output Parameters of BP Neural Networks

The post-fire temperature distribution of RC beams was obtained in Sect. 2.2; the mechanical properties of post-fire reinforced steel and concrete were determined in Sect. 2.3; the shear resistance of post-fire RC beams was calculated in Sect. 2.4. The theoretical shear resistance of post-fire RC beams was calculated using the strength reduction calculation model, and this theoretical value was the target value of neural network.

Due to the high cost of the shear capacity tests of the beam under fire, there are few tests available. Therefore, this paper proposes an alternative method, which uses the shear capacity values calculated according to the Chinese concrete code GB50010-2010 as training data. In this paper, the material strength degradation under fire and fire exposure time are considered. The comparison of the calculated

data with the experimental results is made, good agreement is achieved, hence, it can be used as training data.

The data packet included 7 parameters: beam width b, beam height h, fire exposure time t, sectional area of stirrup A_{sv}, stirrup spacing s, tensile strength of concrete f_t, and concrete cover thickness c. The values of the input layer parameters were b (200–220–250–300 mm), h (400–450–500–550–600–650–700 mm), A_{sv} (100.53, 157, 226.08 mm^2), f_t (2.80, 3.22, 3.50 MPa), s (100, 150, 200 mm), c (25, 35, 45 mm), t (5, 10, 15, 20, 25, 30, 35, 40, 45, 50, 55, 60, 65, 70, 75, 80, 85, 90, 95, 100, 105, 110, 115, 120 min). The output neuron is shear resistance.

4.2 Training and Testing

Neural networks were built using the toolbox on MATLAB R2014b. 384 groups of data for training and testing. The 384 groups of training data are divided into three parts during the network training process: training data (default 70%), validation data (default 15%), test data (default 15%), and data selection is random. In general, the more complex the mapping between input and output, the greater the noise contained in the sample, which requires a large number of training samples. The more the number of training samples, the more the impact of the outliers can be ignored, and the more accurate the training results reflect the inherent laws.

The structural system of the BP neural network is shown in Fig. 6. The structure of the BP neural network (Mar et al. 2016; Moghaddam et al. 2016) consists of input layer, intermediate hidden layer, and output layer. The BP neural network structure designed in this paper has 7 input neurons in the input layer, 25 and 5 hidden neurons in the double hidden layer, and 1 output neuron in the output layer. The symbolic explanations of the input and output layers are given in Sect. 4.2. The network training parameters are set to: the number of training steps is 60, the learning rate is 0.05, the training target is 3000, and the training target is 1e−5.

Here are the network training steps

(1) Initialize the weight and threshold and give the activation function.
(2) The output calculation of the hidden layer and the output layer, and the predicted output of the output layer is obtained according to the weight and the threshold.
(3) Calculate the error between the two based on the predicted output and the expected output.
(4) Determine whether to end the training based on the error. If yes, end the training and get the final predicted output; if not, update the weight and threshold, return to step (2).

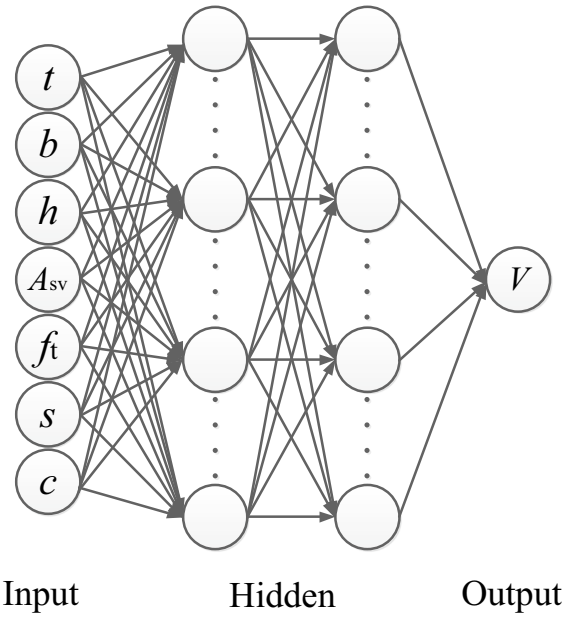

Fig. 6 Construction of BP neural network system.

4.3 Data Normalization

Input/output data needs to be pre-processed before training, which speeds up the convergence of the training network and puts the data into the same order of magnitude for more accurate predicted results. Data normalization is a commonly used data preprocessing method that transforms input/output data into values in the [0,1] interval, and the expression can be calculated as follows:

$$\bar{x}_i = \frac{x_i - x_{\min}}{x_{\max} - x_{\min}} \tag{10}$$

where x_i is input/output data, $x_{\min}$ is minimum range of data change, $x_{\max}$ is maximum range of data change.

The selection of the neural network parameters largely affected the final results. The hidden layer decided the final learning effect. As the number of hidden layers increased, the ability to solve complex problems enhanced. Due to the complexity of the mapping relationship, the increase in the number of hidden layer nodes in the single hidden layer is insufficient to improve network performance. In this study, a double-hidden-layer preceptor was used, which theoretically could solve the majority of complex classification problems. The neurons of the hidden layer adopted a Sigmoid activation transfer function, the output was controlled within [0,1]. After transformation, the overly large absolute value of the net input that would make the neuron output saturate was avoided, and thereby the weight adjustment entered the flat zone of the error cambers. The choice of the number

of hidden layer neurons is a very complicated problem. There is no ideal analytical equation, which needs to be determined according to the designer's experience and many experiments. The method adopted in this paper is to put a small number of neurons at the beginning, and after learning some times, if it is not successful, increase the number of hidden layer neurons until a reasonable number of hidden layer neurons is reached. The output layer neurons use the purein linear function to improve the predicted data accuracy of the network. For training, and a Levenberg-Marquard algorithm was used, which was featured by a fast gradient declining rate and a fewer training steps but occupied more memory (Sarabakha et al. 2017).

The used sigmoid activation function can be described as follows:

$$S(x) = \frac{1}{1 + \exp(-x)} \tag{11}$$

4.4 Testing Result

After the neural network started to run, the MSE declined quickly and finally dropped below 1. These results were acceptable and indicated this prediction model worked well. The R at the training is 0.99996. Since an R closer to 1 suggests the fitting effect is better, this neural network has high generalization ability. As shown in Fig. 7, the error (e) fluctuation in between the target values V_{target} based on theoretical computation and the predicted values V_{output} based on neural network does not exceed 2%. This BP neural network showed high simulation and learning ability, and thus can be used to predict the shear resistance of post-fire RC beams.

5 Prediction Results and Discussion

After training, the 96 groups of data were used for prediction, and the predicted results were shown in Table 2. The predicted values match well with the target values, with relative errors around 1.63%. In order to prove the feasibility of the method, the trained network was used to predict the experimental data in Ref. (Xu et al. 2013). The prediction result was 120.60 and the relative error was 0.5%. Clearly, the neural network model had high computational accuracy and generalization ability and could well reflect the relation between the shear resistance of post-fire reinforced steel beams and the different influence factors. Thus, this model can be used to analyze and predict.

Then the effects of different parameters on the shear resistance of post-fire RC beams were investigated with this neural network.

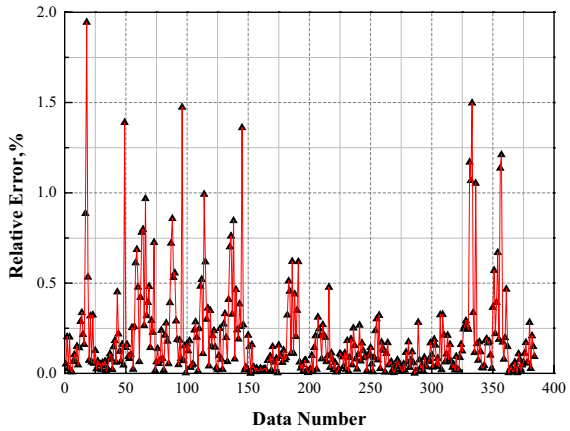

Fig. 7 Relative error between the target and output shear resistance.

6 Parametrical Study on Shear Resistance Using Machine Learning

As the results from training, testing and prediction are satisfactory, so the machine is used to assess the effect of different parameters on the shear resistance. In the parametric analysis, the appropriate beams are selected to analyze the impact of each parameter. The values of different key parameters were input into the machine for the shear resistance predictions. Based on prediction results, the effects of the parameters on shear resistance were further studied, the results are show as follows:

6.1 Effects of Beam Width *b*

The effect of beam width b on shear resistance was studied. The input parameters were $b = 200$, 220, 250 mm, $h = 500$ mm, $A_{sv} = 100.53$ mm^2, $f_t = 2.80$ MPa, $s = 150$ mm, $c = 25$ mm, $t = 0$, 5, 10, 15, 20, 25, 30, 35, 40, 45, 50, 55, 60, 65, 70, 75, 80, 85, 90, 95, 100, 105, 110, 115, 120 min. The effect of beam breadth on the shear resistance of beams was illustrated in Fig. 8. Clearly, the shear resistance was weakened with the prolonging of fire exposure time but was strengthened with the increase of beam breadth.

6.2 Effects of Beam Height h

The effect of beam height h on shear resistance was studied. The input parameters were $b = 200$, $h = 400$, 450, 500 mm, $A_{sv} = 157$ mm^2, $f_t = 2.80$ MPa, $s = 150$ mm, $c = 25$ mm, $t = 5$, 10, 15, 20, 25, 30, 35, 40, 45, 50, 55, 60, 65, 70, 75, 80, 85, 90, 95, 100, 105, 110, 115, 120 min. The effect of beam height on the shear resistance of beams is illustrated in Fig. 9. Clearly, the shear resistance was weakened with the prolonging of fire exposure time but was strengthened with the increase of beam height.

Table 2 Predicted data.

No.	t (min)	b (mm)	h (mm)	A_{sv} (mm^2)	f_t (MPa)	s (mm)	c (mm)	V_{target} (kN)	V_{output} (kN)	e (%)
1	5	220	500	100.53	2.8	150	25	307.07	305.58	0.48
2	10	220	500	100.53	2.8	150	25	302.59	301.56	0.34
3	15	220	500	100.53	2.8	150	25	296.89	297.66	0.26
4	20	220	500	100.53	2.8	150	25	291.69	293.88	0.75
5	25	220	500	100.53	2.8	150	25	287.58	290.23	0.92
6	30	220	500	100.53	2.8	150	25	283.85	286.73	1.01
7	35	220	500	100.53	2.8	150	25	280.76	283.41	0.95
8	40	220	500	100.53	2.8	150	25	278.54	280.32	0.64
9	45	220	500	100.53	2.8	150	25	276.6	277.5	0.32
10	50	220	500	100.53	2.8	150	25	275.13	274.98	0.05
11	55	220	500	100.53	2.8	150	25	273.74	272.84	0.33
12	60	220	500	100.53	2.8	150	25	272.44	271.09	0.5
13	65	220	500	100.53	2.8	150	25	271.24	269.75	0.55
14	70	220	500	100.53	2.8	150	25	270.11	268.79	0.49
15	75	220	500	100.53	2.8	150	25	269.08	268.11	0.36
16	80	220	500	100.53	2.8	150	25	268.17	267.5	0.25
17	85	220	500	100.53	2.8	150	25	267.39	266.63	0.29
18	90	220	500	100.53	2.8	150	25	266.72	265.07	0.62
19	95	220	500	100.53	2.8	150	25	262.29	262.35	0.02
20	100	220	500	100.53	2.8	150	25	256.13	258.15	0.79
21	105	220	500	100.53	2.8	150	25	250.33	252.44	0.84
22	110	220	500	100.53	2.8	150	25	244.88	245.56	0.28
23	115	220	500	100.53	2.8	150	25	239.64	238.04	0.67
24	120	220	500	100.53	2.8	150	25	234.13	230.32	1.63
.	.	.	.	.	.	.	.	.	.	.
.	.	.	.	.	.	.	.	.	.	.
.	.	.	.	.	.	.	.	.	.	.
73	5	300	650	100.53	2.8	150	25	517.84	512.19	1.09
74	10	300	650	100.53	2.8	150	25	513.44	506.12	1.43
75	15	300	650	100.53	2.8	150	25	505.3	499.1	1.23
76	20	300	650	100.53	2.8	150	25	494.87	491.12	0.76
77	25	300	650	100.53	2.8	150	25	484.59	482.28	0.48
78	30	300	650	100.53	2.8	150	25	474.97	472.8	0.46
79	35	300	650	100.53	2.8	150	25	463.3	463.05	0.05
80	40	300	650	100.53	2.8	150	25	452.13	453.5	0.3
81	45	300	650	100.53	2.8	150	25	442.64	444.66	0.46
82	50	300	650	100.53	2.8	150	25	433.83	436.84	0.69
83	55	300	650	100.53	2.8	150	25	427.54	430.04	0.59
84	60	300	650	100.53	2.8	150	25	420.82	423.87	0.73
85	65	300	650	100.53	2.8	150	25	414.41	417.6	0.77
86	70	300	650	100.53	2.8	150	25	408.41	410.47	0.5
87	75	300	650	100.53	2.8	150	25	402.16	401.9	0.07
88	80	200	650	100.53	2.8	150	25	388.9	391.68	0.72
89	85	200	650	100.53	2.8	150	25	375.81	380.04	1.13
90	90	200	650	100.53	2.8	150	25	367.03	367.55	0.14
91	95	200	650	100.53	2.8	150	25	353.82	354.97	0.33
92	100	200	650	100.53	2.8	150	25	345.42	343.07	0.68
93	105	200	650	100.53	2.8	150	25	333.43	332.49	0.28
94	110	200	650	100.53	2.8	150	25	325.89	323.66	0.68
95	115	200	650	100.53	2.8	150	25	319.42	316.84	0.81
96	120	200	650	100.53	2.8	150	25	314.84	312.14	0.86

V_{target} and V_{output} were the target value and predicted value of the reinforced concrete, respectively; $e = \left|V_{target} - V_{output}\right|/V_{target}$.

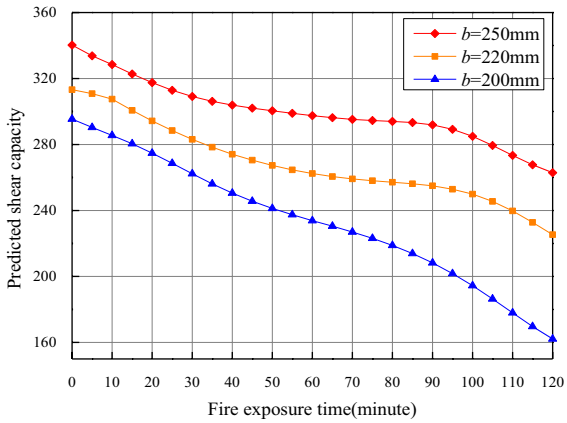

Fig. 8 Effect of beam width *b* on shear resistance of beams.

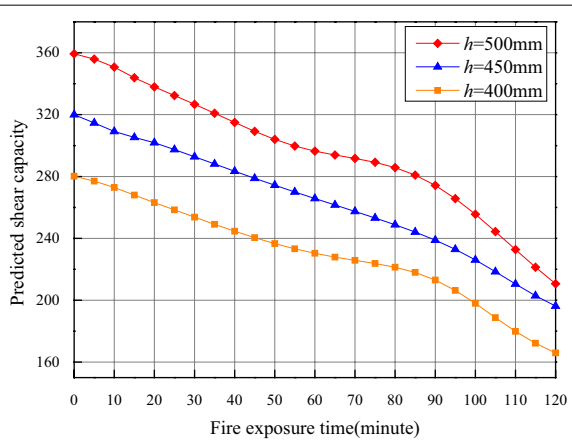

Fig. 9 Effect of beam height *h* on shear resistance of beams.

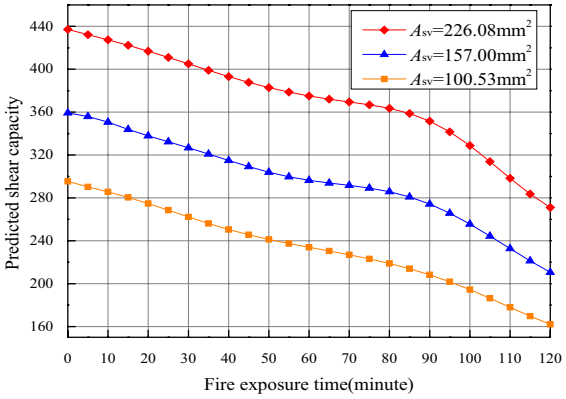

Fig. 10 Effect of stirrup sectional area A_{sv} on shear resistance of beams.

6.3 Effects of Stirrup Sectional Area A_{sv}

The effect of stirrup sectional area A_{sv} on shear resistance was studied. The input parameters were $b=200$ mm, $h=500$ mm, $A_{sv}=100.53$, 157, 226.08 mm^2, $f_t=2.80$ MPa, $s=150$ mm, $c=25$ mm, $t=5$, 10, 15, 20, 25, 30, 35, 40, 45, 50, 55, 60, 65, 70, 75, 80, 85, 90, 95, 100, 105, 110, 115, 120 min. The effect of stirrup sectional area on the shear resistance of beams was illustrated in Fig. 10. Clearly, the shear resistance was weakened with the prolonging of fire exposure time but was strengthened with the enlargement of stirrup sectional area.

6.4 Effect of Stirrup Spacing *s*

The effect of stirrup spacing s on shear resistance was studied. The input parameters were $b=200$ mm, $h=500$ mm, $A_{sv}=157$ mm^2, $f_t=2.80$ MPa, $s=100$, 150, 200 mm, $c=25$ mm, $t=5$, 10, 15, 20, 25, 30, 35, 40, 45, 50, 55, 60, 65, 70, 75, 80, 85, 90, 95, 100, 105, 110, 115, 120 min. The effect of stirrup spacing on the shear resistance of beams was illustrated in Fig. 11. Clearly, the shear resistance was weakened with the prolonging of fire exposure time but was strengthened with the reduction of stirrup spacing.

6.5 Effect of Concrete Tensile Strength f_t

The effect of concrete tensile strength f_t on shear resistance was studied. The input parameters were $b=200$ mm, $h=500$ mm, $A_{sv}=100.53$ mm^2, $f_t=2.80$, 3.22, 3.50 MPa, $s=150$ mm, $c=25$ mm, $t=5$, 10, 15, 20, 25, 30, 35, 40, 45, 50, 55, 60, 65, 70, 75, 80, 85, 90, 95, 100, 105, 110, 115, 120 min. The effect of concrete tensile strength on the shear resistance of beams was shown in Fig. 12. Clearly, the shear resistance was weakened with the prolonging of fire exposure time but was strengthened with the increase of concrete tensile strength.

6.6 Effect of Concrete Cover Thickness *c*

The effect of concrete cover thickness c on shear resistance was studied. The input parameters were $b=200$ mm, $h=500$ mm, $A_{sv}=157$ mm^2, $f_t=2.80$ MPa, $s=150$ mm, $c=25$, 35 mm, $t=5$, 10, 15, 20, 25, 30, 35, 40, 45, 50, 55, 60, 65, 70, 75, 80, 85, 90, 95, 100, 105, 110, 115, 120 min. The effect of concrete cover thickness on the shear resistance of beams is illustrated in Fig. 13. Clearly, the shear resistance was weakened with the prolonging of fire exposure time. Within 90 min, the shear resistance of the concrete with cover thickness of $c=25$ mm is greater than that of the beams with $c=35$ mm due to its larger effective height. After 90 min, the stirrup temperature of the $c=25$ mm beam caused the strength reduction and significant decline of shear resistance, but the stirrup of the $c=35$ mm beam did not have some degree of decline due to its thicker cover, so the shear resistance of the $c=25$ mm beam was smaller than that of the $c=35$ mm beam.

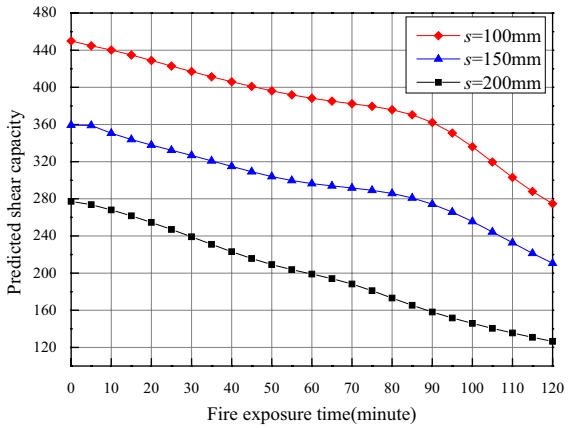

Fig. 11 Effect of stirrup spacing *s* on shear resistance of beams.

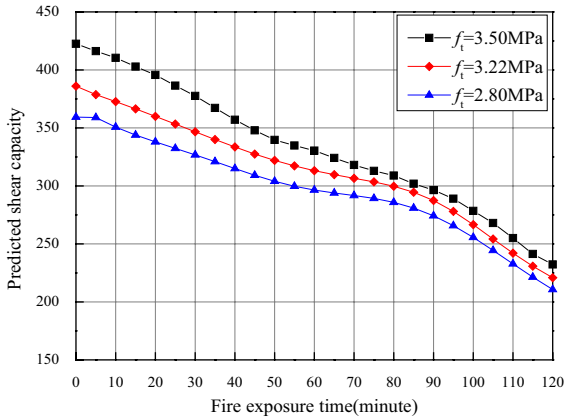

Fig. 12 Effect of concrete tensile strength f_t on shear resistance of beams.

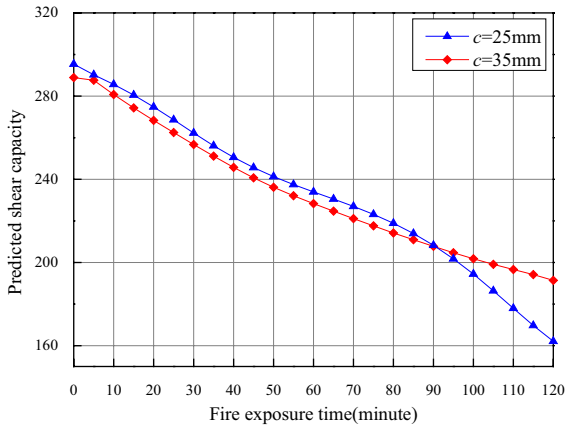

Fig. 13 Effect of concrete cover thickness *c* on shear resistance of beams.

From above As we know, the strength of materials of reinforced concrete decreases with increasing temperature, and the shear capacity of the beam decreases with the increase of fire time. It is known from the Eq. (8) of the Chinese Code GB (2010) that the shear resistance of reinforced concrete beams comes from two components: concrete and stirrups, and most of the shear capacity is resisted by the stirrups at normal temperature. From Eq. (8), it can be seen that, the shear capacity is proportional to the beam width, beam height, stirrup area, concrete tensile strength, and inversely proportional to stirrup spacing. Because the thermal properties of concrete and steel are different, the strength reduction are also different. As the fire time increases, the strength of the steel decreases dramatically. The beam with a small concrete cover thickness begins to reduce the strength of the steel after about 90 min of fire, and the shear capacity dominated by the stirrup increases. However, for the temperature of beams with large concrete cover thickness stirrup strength reduce slowly. Therefore, the shear capacity of beams with smaller concrete cover thickness is lower than that of beams with larger concrete cover thickness.

6.7 Test Result Discussion

In the study of Erdem (2015), the flexural capacity decreased sharply before the fire exposure time was 30 min which is quite different from that of this paper. This is because the flexural capacity is affected more by the longitudinal reinforcement located in the tension zone of the beams than by the concrete. Thus, when the beams are exposed to fire, the flexural capacity appears to decrease more rapidly than the shear capacity. Further, since the shear strength of beams is resisted by concrete and shear reinforcement, the decrease in shear capacity due to fire exposure show a difference in concrete and shear reinforcement. Figure 2 shows the heat transferring result. It can be seen that, in the first 60 min, although the atmosphere temperature sharply increases to 800 °C, the concrete temperature after 60 min only increase to 200 °C for most area of the beam, and the temperature of the some area of the shear links increase to 600 °C, the temperature in the majority area are still around 200 °C. However, to the contrast, the longitudinal bar temperature has increase to around 900 °C. Therefore, the flexural capacity of the beams dropped sharply due to the degradation of the longitudinal bars, but the shear capacity still maintains for high level in the first hour.

7 Conclusions

In this paper, a double hidden layer BP neural network model was established. The neural network model was trained, tested and validated using the data obtained from the post-fire residual shear resistance model. Then, the

machine learning was employed to investigate the effects of beam width, beam height, stirrup sectional area, stirrup spacing, concrete tensile strength, concrete cover thickness, and fire exposure time on the shear resistance of beams. This method integrated the advantages of finite element simulation, theoretical analysis, and machine learning using BP neural network, and could quickly and effectively predict the shear resistance of RC beams after fire, following conclusions are drawn:

1. The post-fire reinforced concrete beams can be evaluated by the residual shear capacity model accurately.
2. The predicted shear resistance using neural network match well with the target values, and the errors from the testing data were all around 1.63%, indicating the BP ANN is feasible for predicting the shear resistance of post-fire RC beams.
3. The shear resistance of RC beams was strengthened with the increase of beam width, beam height, stirrup sectional area, and concrete tensile strength. In addition, the shear resistance was weakened with the rise of fire exposure time or stirrup spacing.
4. At different stage of the fire growth, the effect of the concrete cover thicknesses is different, the effect would change after a certain time point.

Acknowledgements
This research was financially supported by the Foundation of China Scholarship Council (No. 201805975002) National Natural Science Foundation of China (Grant NO. 51378238), Science and Technological Planning Project of Ministry of Housing and Urban–Rural Development of the People's Republic of China (No. 2017-K9-047). The authors wish to acknowledge the sponsors. However, any opinions, findings, conclusions and recommendations presented in this paper are those of the authors and do not necessarily reflect the views of the sponsors.

Authors' contributions
BC and FF designed the research methodology; LFX performed the analysis, LFX and FF draft the manuscript; BC and FF reviewed the manuscript; LFX and FF revised the final manuscript. All authors read and approved the final manuscript.

Funding
Funder: Foundation of China Scholarship Council. Award number 201805975002. Funder: National Natural Science Foundation of China. Award number 51378238. Funder: Science and Technological Planning Project of Ministry of Housing and Urban–Rural Development of the People's Republic of China. Award number 2017-K9-047.

Availability of data and materials
The data used to support the findings of this study are available from the authors upon request.

Competing interests
The authors declare that they have no competing interests.

Author details
[1] School of Civil Engineering, Jilin Jianzhu University, Changchun 130118, Jilin, China. [2] School of Mathematics, Computer Science and Engineering, City, University of London, London, UK.

Received: 20 March 2019 Accepted: 11 July 2019
Published online: 09 September 2019

References

Abbasi, A., & Hogg, P. J. (2005). Prediction of the failure time of glass fiber reinforced plastic reinforced concrete beams under fire conditions. *Journal of Composites for Construction, 9*(5), 450–457.
Annerel, E., & Taerwe, L. (2011). Evolution of the strains of traditional and self-compacting concrete during and after fire. *Materials and Structures, 44*(8), 1369–1380.
Bengar, H. A., Abdollahtabar, M., & Shayanfar, J. (2016). Predicting the ductility of RC beams using nonlinear regression and ANN. *Iranian Journal of Science & Technology Transactions of Civil Engineering, 40*(4), 1–14.
BSI. (2004). *BS EN 1992-1-2:2004, Eurocode 2—Design of concrete structures-part 1–2: General rules-structural fire design. Structural fire design*. London: BSI.
BSI. (2013). *BS ENV 1994-1-2, Eurocode 4—Design of composite steel and concrete structures—part 1–2: General rules. Structural fire design*. London: BSI.
Chowdhury, E. U., & Bisby, L. A. (2008). Residual behavior of fire-exposed reinforced concrete beams prestrengthened in flexure with fiber-reinforced polymer sheets. *Journal of Composites for Construction, 12*(1), 61–68.
El-Fitiany, S. F., & Youssef, M. A. (2017). Fire performance of reinforced concrete frames using sectional analysis. *Engineering Structures, 142,* 165–181.
Erdem, H. (2010). Prediction of the moment capacity of reinforced concrete slabs in fire using artificial neural networks. *Advances in Engineering Software, 41*(2), 270–276.
Erdem, H. (2015). Predicting the moment capacity of RC beams exposed to fire using ANNs. *Construction and Building Materials, 101,* 30–38.
Felicetti, R., Gambarova, P. G., & Meda, A. (2009). Residual behavior of steel rebars and R/C sections after a fire. *Construction and Building Materials, 23*(12), 3546–3555.
Fu, F. (2016). *Structural analysis and design to prevent disproportionate collapse*. Boca Raton: CRC Press.
GB. (2010). GB 50010-2010: Code for design of concrete structures. GB, China, Beijing.
Gupta, G. P., Nair, R. R., & Jeyanthi, R. (2017). An ANN based SpO2 measurement for clinical management systems. *Energy Procedia, 117,* 393–400.
Hu, C., Xu, Y., Luo, Y., Zheng, Y., & Lin, B. (2014). Experimental study on the tensile strength of concrete after high temperature. *Journal of Huaqiao University (Natural Science), 35*(2), 196–201.
ISO (International Organisation for Standardisation). (1999). *ISO 834-1: Fire resistance tests—elements of building construction. Part 1: General requirements*. Geneva: ISO.
Keskin, R. S. O., & Arslan, G. (2013). Predicting diagonal cracking strength of RC slender beams without stirrups using ANNs. *Computers & Concrete, 12*(5), 697–715.
Kurtgoz, Y., Karagoz, M., & Deniz, E. (2018). Biogas engine performance estimation using ANN. *Engineering Science and Technology, an International Journal, 20*(6), 1563–1570.
Leśniak, A., & Juszczyk, M. (2018). Prediction of site overhead costs with the use of artificial neural network based model. *Archives of Civil & Mechanical Engineering, 18*(3), 973–982.
Liu, Y., Li, H., Wang, X., & Wang, Q. (2000). TFIEILD-a software package for temperature field analysis of reinforced concrete members exposed to fire. *Journal of Shenyang Architectural and Civil Engineering Institute, 16*(4), 251–253.
Lou, Y., Wu, W., & Zhuang, J. (2017). The prediction to the flexural capacity of self-compacting concrete beam base on BP neural network. *Journal of Changchun Institute of Technology (Natural Science), 18*(1), 34–36.
Mar, B., Md, R., & Fumo, N. (2016). *Prediction of residential building energy consumption: A neural network approach, Energy*. Amsterdam: Elsevier.
Marugán, A. P., Márquez, F. P. G., Perez, J. M. P., & Ruiz-Hernández, D. (2018). A survey of artificial neural network in wind energy systems. *Applied Energy, 228,* 1822–1836.
Mashrei, M. A., Abdulrazzaq, N., Abdalla, T. Y., & Rahman, M. S. (2010). Neural networks model and adaptive neuro-fuzzy inference system for predicting the moment capacity of ferrocement members. *Engineering Structures, 32*(6), 1723–1734.
Moghaddam, A. H., Moghaddam, M. H., & Esfandyari, M. (2016). Stock market index prediction using artificial neural network. *Journal of Economics, 21,* 89–93.

Molkens, T., Coile, R. V., & Gernay, T. (2017). Assessment of damage and residual load bearing capacity of a concrete slab after fire: applied reliability-based methodology. *Engineering Structures, 150,* 969–985.
Mossalam, A., & Arafa, M. (2017). Using artificial neural networks (ANN) in projects monitoring dashboards' formulation. *HBRC Journal, 14,* 385–392.
Naser, M., Abulebdeh, G., & Hawileh, R. (2012). Analysis of RC T-beams strengthened with CFRP plates under fire loading using ANN. *Construction and Building Materials, 37*(12), 301–309.
Ožbolt, J., Bošnjak, J., Periškić, G., & Sharma, A. (2014). 3D numerical analysis of reinforced concrete beams exposed to elevated temperature. *Engineering Structures, 58,* 166–174.
Rumelhart, D. E., Hinton, G. E., & Williams, R. J. (1986). Learning Internal Representations by Error Propagation. In D. E. Rumenhart & J. L. McCelland (Eds.), *Parallel distributed processing: Explorations in the microstructure of cognition* (pp. 318–362). Cambridge: MIT Press.
Sarabakha, A., Imanberdiyev, N., Kayacan, E., Khanesar, M., & Hagras, H. (2017). Novel levenberg–marquardt based learning algorithm for unmanned aerial vehicles. *Information Sciences*. https://doi.org/10.1016/j.ins.2017.07.020.
Sarro, L. M., Fernández, C. S., Giménez, A., & Marín, D. L. (2003). *Automated classification of light curves using ANNs, highlights of Spanish astrophysics III* (pp. 511–540). Netherlands: Springer.
Staub, S., Karaman, E., Kaya, S., Karapınar, H., & Güven, E. (2015). Artificial neural network and agility. *Procedia-Social and Behavioral Sciences, 195,* 1477–1485.
Viotti, P., Liuti, G., & Genova, P. D. (2002). Atmospheric urban pollution: applications of an artificial neural network (ANN) to the city of perugia. *Ecological Modelling, 148*(1), 27–46.
Xu, Y., Peng, X., Dong, Y., Luo, Y., & Lin, B. (2015). Experimental study on shear behavior of reinforced concrete beams strengthened with CFRP sheet after fire. *Journal of Building Structures, 36*(2), 123–132.
Xu, Y., Wu, B., Wang, R., Jiang, M., & Luo, Y. (2013). Experimental study on residual performance of reinforced concrete beams after fire. *Journal of Building Structures, 34*(8), 20–29.
Yang, Z. (2008). Numerical simulation of temperature field of reinforced concrete members under fire. (Master dissertation. Central South University).
Yu, Z., Zi, W., Kuang, Y., & Zhang, L. (2012). Influences of temperature and time on concrete cubic compressive strength. *Fire Science and Technology, 2,* 111–114.
Zhou, M., & Ke, G. (2016). Experiment and its prediction artificial neural networks model study on the compressive strength of waste glass concrete. *Concrete, 4,* 54–56.
Zhu, D. (2011). Analysis of thermo-elastic-plastic on reinforced concrete structures subjected to fire. (Doctoral dissertation, Harbin Engineering University).

Publisher's Note